Electrical properties of $NiS_{2-x}Se_x$ single crystals: From Mott insulator to paramagnetic metal

X. Yao* and J. M. Honig
Department of Chemistry, Purdue University, West Lafayette, Indiana 47907-1393

T. Hogan and C. Kannewurf
Department of Electrical Engineering and Computer Science, Northwestern University, Evanston, Illinois 60208-3118

J. Spałek
Institute of Physics, Jagiellonian University, Ulica Reymonta 4, 30-059 Kraków, Poland†
and Department of Physics, Purdue University, West Lafayette, Indiana 47907-1396

(Received 6 June 1995; revised manuscript received 29 March 1996)

Electrical resistivity (ρ) and Seebeck-coefficient measurements (α) are reported for $NiS_{2-x}Se_x$ single crystals in the range $0 \leqslant x \leqslant 0.71$. There is a general trend toward increasing metallicity with increasing x. In the range $0.38 \leqslant x \leqslant 0.51$ a pronounced rise of ρ with temperature (T) is observed where the antiferromagnetic insulating (or antiferromagnetic metallic) phase changes over to the paramagnetic insulating phase. The analysis of α vs T curves suggests that in the low-temperature insulating state both holes and electrons participate in charge transport. It is emphasized that the many changes in electrical characteristics occur without significant alterations in the pyrite crystal structure, and that physical properties are greatly altered solely by adjustment of the anion sublattice while the cation sublattice remains intact. The results concerning electrical transport for the samples with $0.38 \leqslant x \leqslant 0.55$ are interpreted qualitatively on the basis of an onset of the Hubbard splitting into subbands at the transition to the insulating (semiconducting) state, which takes place in the temperature interval (50–100 K) upon heating the samples. The metallic state close to the metal-semiconductor boundary is viewed as being an antiferromagnetic semimetal, with an anisotropic Slater gap. [S0163-1829(96)06247-9]

I. INTRODUCTION

There is continuing interest in systems that undergo metal-insulator transitions (MIT's). Studies of this phenomenon have generally been confined to transition-metal oxides where such effects are primarily encountered. The related system $NiS_{2-x}Se_x$ is unusual in two respects: first, it is a chalcogenide which exhibits metal-insulator transitions between magnetically ordered phases; second, its properties can be drastically altered by varying the composition of the anion sublattice, while the cation sublattice remains intact. This latter circumstance is encountered only very rarely and is very important, since the observed metal-insulator transitions involve mainly the $3d$ states of cations. In this manner, the disorder effects are minimized and the transition is induced solely by the electron-electron interactions. Earlier work reported in the literature,[1–23] as well as the present investigation on $NiS_{2-x}Se_x$, were motivated by the fact that NiS_2 is a magnetic insulator, whereas $NiSe_2$ is a good metal; these two compounds form isostructural solid solutions accurately obeying Vegard's law[2] over the entire composition range $0 \leqslant x \leqslant 2$. One therefore anticipates a range of x values where the alloy displays intermediate anomalous electrical characteristics; this is indeed the case for $0.38 \leqslant x \leqslant 0.55$. The most important feature in this respect is the opening of a Mott-Hubbard gap when the temperature is increased, which provides an unambiguous signature for Mott localization, as elaborated below.

There have been several prior investigations of the electrical properties of $NiS_{2-x}Se_x$. Pioneering and early studies were carried out on single crystals grown by vapor transport techniques;[1,3,11] in later measurements sintered specimens[1,19,20] were employed. While all of these studies are qualitatively concordant there remain many questions. Difficulties of electrical measurements on polycrystalline materials are well known. Furthermore, single crystals used in physical measurements to date were grown by chemical vapor transport techniques. As has been documented some time ago,[24] the inclusion of carrier gases as a dopant impurity at the 100–600-ppm level is unavoidable in such a procedure. This seriously affects the transport characteristics of the host, at least in the range of compositions with $x < 0.6$, where the material displays semiconducting characteristics. We therefore felt it appropriate to carry out a new set of measurements on the $NiS_{2-x}Se_x$ system (with $x \leqslant 0.71$), involving single crystals grown in a Te flux, whereby the unintentional doping problem can be avoided. In such a situation the opening of the Mott-Hubbard gap, particularly at finite temperature, is not hindered by extrinsic features in the conductivity.

II. EXPERIMENTAL TECHNIQUES

Polycrystalline $NiS_{2-x}Se_x$ was synthesized by heating stoichiometric amounts of Ni, S, and Se at 730 °C for several days in an evacuated silica tube. Single crystals were grown from these starting materials using Te as a flux, according to a procedure described elsewhere in detail;[21,22] this method

was originally employed in the growth of RuS_2 (Ref. 25) and FeS_2 (Ref. 26) single crystals. It was established via x-ray dispersive analysis that no Te is detectable in the single crystals obtained by this method. The presence of very small amounts of Te would in any case not seriously affect the electrical properties.

The electrical resistivity (ρ) was studied primarily by use of the van der Pauw procedure;[27] contacts were formed by drying silver epoxy onto copper wires attached by silver paint to samples approximately 1 mm^3 in dimension. The temperature was monitored with a calibrated carbon-glass thermometer and regulated with a temperature controller. Data collection was automated. There is some uncertainty in the absolute value of ρ because the correction for the ratio of resistances, f, cited in Ref. 27, is not precisely known; for our samples it fell in the range $1 \geq f \geq 0.8$. For simplicity we set $f=1$; our conclusions and the comparison of our data with earlier results remain essentially unaffected by this choice. In a few instances a four-probe technique was employed; in this case thin gold wires were bonded to the crystals with gold paste.

Thermoelectric measurements were carried out under computer control[28] using the slow-ac technique developed by Chaikin and Kwak.[29] Two samples were placed in parallel between two individually heated quartz blocks; the temperature gradient of ~ 1 K was software adjustable. Data were taken while the samples were warmed incrementally from 4.2 to 300 K, and equilibrated at a series of closely spaced temperatures. The total processing times were of the order of 60 h per run. Corrections were applied for the thermal voltages of the gold electrodes. Below 30 K the data became unreliable because of interference by the phonon-drag peak of Au.

All measurements were carried out on as-grown specimens. It has been documented for NiS_2 (Refs. 5,6) that relatively small changes in cation/anion ratios do somewhat affect the electrical characteristics. A similar effects was observed by us in comparing the electrical characteristics of untreated $NiS_{2-x}Se_x$, $x=0.51$, with a sample that had been annealed in a sealed quartz ampoule at 700 °C for 7 days. The detailed investigation of these effects will be the subject of a future study.

III. EXPERIMENTAL RESULTS

The variation in resistivity (ρ) with temperature (T) is shown in Figs. 1–5 for various ranges of x in $NiS_{2-x}Se_x$. A summary is shown in Figs. 6(a) and 6(b) as plots of $\log_{10}\rho$ vs T for the entire concentration range under investigation.

Broadly speaking, one can discern four regimes. (a) The range $0 \leqslant x \lesssim 0.24$: here ρ exceeds 10^3 Ω cm as $T \to 0$; ρ passes through a small maximum between 50 and 130 K and then drops steadily with rising temperature. For $x=0.38$, $\rho(0)$ is approximately 10^2 Ω cm; for temperatures both below and above the region of the shallow maximum the resistivity shows an exponential T dependence, as discussed below. (b) In the composition range $0.40 \lesssim x \lesssim 0.51$ the resistivity is small both near 0 K and above 150 K. The material exhibits a marked maximum at an intermediate temperature T_m for which $\rho(T_m)/\rho(0)$ can approach a factor of 10^3. (c) In the range $0.55 \lesssim x \lesssim 0.58$ the features are rather like those of (b) except that the resistivities are much lower and the peaks in the resistivity curves decrease in magnitude and are broadened. (d) For $x \gtrsim 0.6$ the alloy displays metallic characteristics: ρ rises monotonically with T.

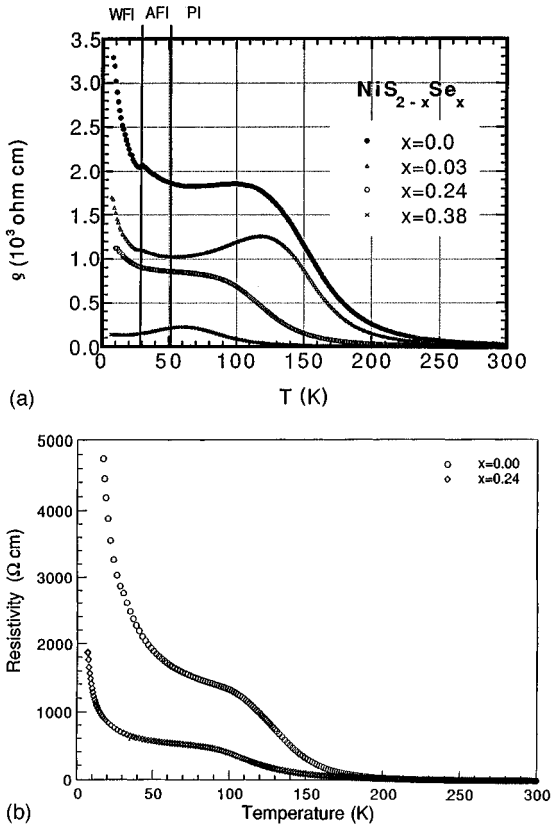

FIG. 1. (a) Plots of resistivity ρ vs temperature T for single crystals of $NiS_{2-x}Se_x$ in the composition range $0 \leqslant x \leqslant 0.24$. Data taken using the van der Pauw technique. The regions of the various phases of Fig. 9 are indicated at the top of the diagram. (b) Four-probe resistivity measurements of single crystals of $NiS_{2-x}Se_x$ with $x=0$, 0.24.

The thermoelectric data are shown in Figs. 7 and 8 for samples in the composition range $0 \leqslant x \leqslant 0.44$ and $0.51 \leqslant x \leqslant 0.71$, respectively. The quality of data below 30 K is questionable because the corrections for the contribution

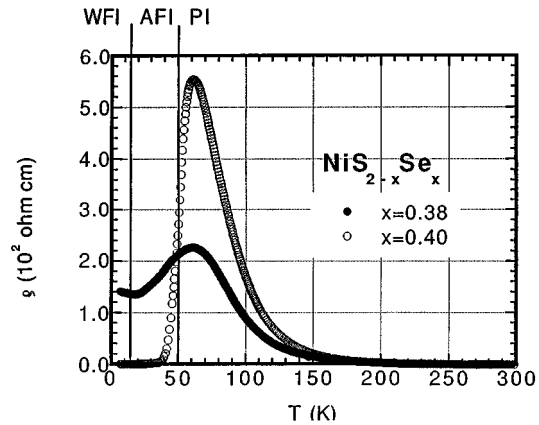

FIG. 2. ρ vs T for single crystal $NiS_{2-x}Se_x$ for $x=0.38$, 0.40. The regions of the various phases of Fig. 9 are indicated at the top of the diagram.

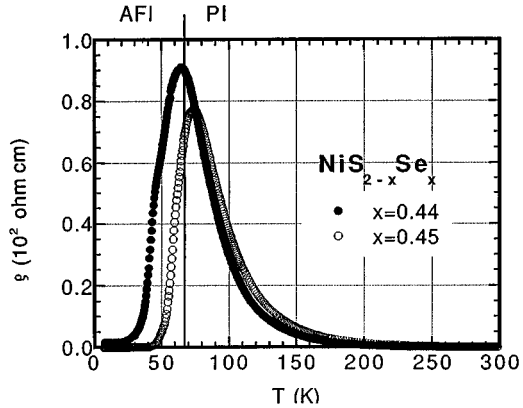

FIG. 3. ρ vs T for single crystal $NiS_{2-x}Se_x$ for $x=0.44$, 0.45. The regions of the various phases of Fig. 9 are indicated at the top of the diagram.

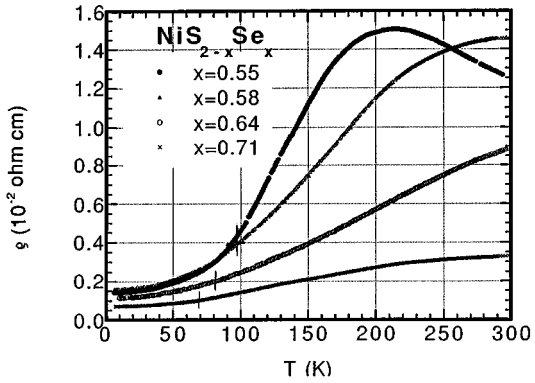

FIG. 5. ρ vs T for single crystal $NiS_{2-x}Se_x$ in the composition range $0.55 \leqslant x \leqslant 0.71$. The vertical bars indicate the temperature of the AFM-PM transition shown in Fig. 9.

to α of the gold leads becomes uncertain due to the phonon-drag effect in gold. The measurements in Fig. 7 show a changeover in sign for some samples in the lower- and higher-temperature range and exhibit a peak at a temperature T_m for all specimens at intermediate temperatures. The remaining measurements in Fig. 8 all fall in the negative range of α for $T>30$ K and are numerically small.

Concerning resistivity, the above qualitative features are in consonance with those reported in the literature.[3,11,19] The present resistivities are, however, higher by as much as two orders of magnitude than those reported earlier, presumably reflecting the absence of unintentional dopants that were introduced by use of chemical vapor transport techniques. The variations of α with T are similar to those reported earlier,[11] except that the present numerical values are smaller by nearly a factor of five. This again is consistent with the greater purity of our samples.

A. Resistivity data

We now attempt to correlate the resistivity measurements with phase diagrams cited in the literature;[4–7,9,13,17,20] these are based on heat capacity, x-ray and neutron scattering, magnetic susceptibility, ^{77}Se NMR, and ^{61}Ni Mössbauer data. These phase diagrams are in qualitative agreement with one another, but differ in the exact placement of the phase boundaries on the T vs x plane. A composite sketch which interpolates with some fairing between the various published diagrammatic representations is provided in Fig. 9; the dashed lines and horizontal bars indicate uncertainties or differences in the findings concerning the location of phase boundaries. One should note the large variety of different phases that have been reported; for a key to the abbreviations

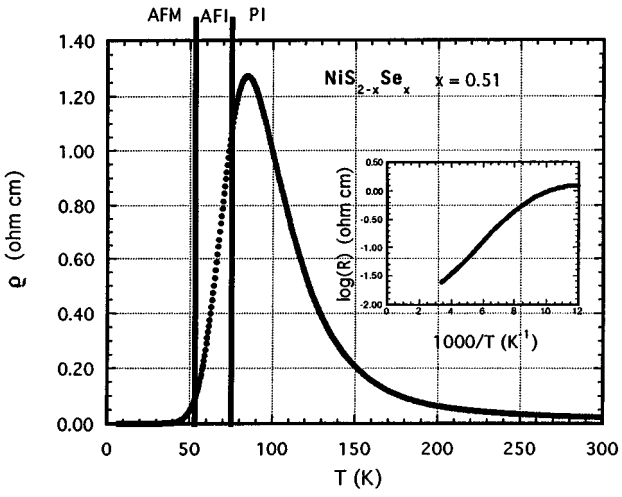

FIG. 4. ρ vs T for single crystal $NiS_{1.49}Se_{0.51}$. Inset shows plot of $\log_{10}\rho$ vs $1/T$. The regions of the various phases of Fig. 9 are indicated at the top of the diagram.

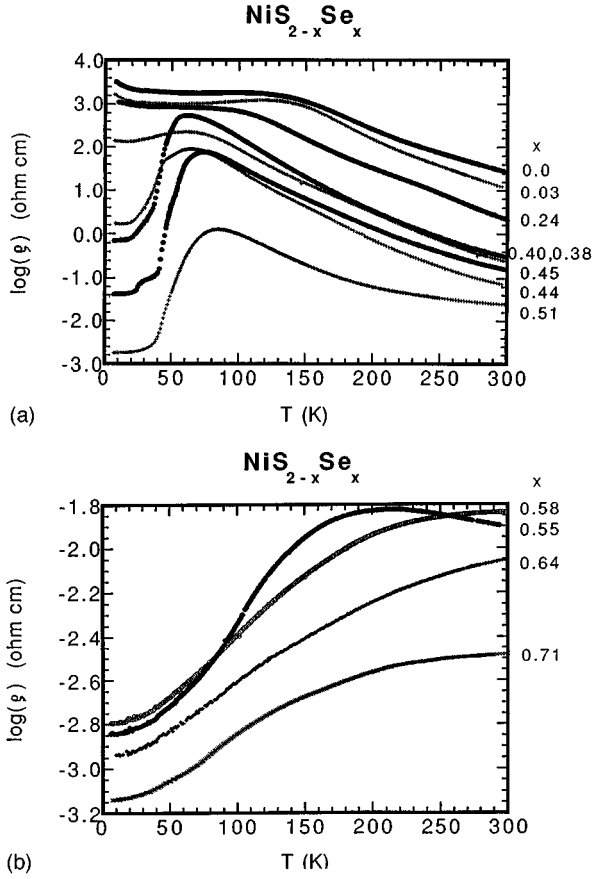

FIG. 6. (a) Summary of experimental resistivity measurements as plots of $\log_{10}\rho$ vs T for the composition range $0 \leqslant x \leqslant 0.51$. (b) Summary of experimental resistivity measurements as plots of $\log_{10}\rho$ vs T for the composition range $0.55 \leqslant x \leqslant 0.71$.

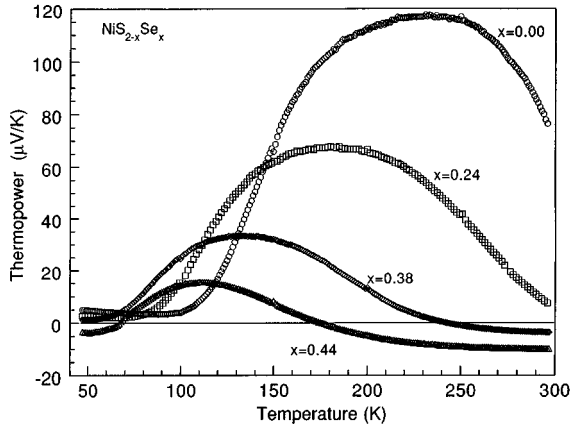

FIG. 7. Thermoelectric properties for $NiS_{2-x}Se_x$ in the composition range $0 \leqslant x \leqslant 0.44$.

see the figure caption. Consistent with earlier reports, magnetic ordering gives way to paramagnetism at higher temperatures and an increasing degree of metallicity arises as the Se/S ratio is increased.

The resistivity curves are subdivided into categories according to sample composition, which, in turn, determines the type of $\rho(T)$ behavior.

(a) $0 \leqslant x \lesssim 0.24$: Representative curves are shown in Fig. 1(a). With rising $T < 30$ K there is an initial drop in ρ, in the range where the weakly ferromagnetic insulator (WFI) phase (actually, a canted antiferromagnetic structure) is stable. For the fcc cationic sublattice a small anomaly is observed at the transition to the antiferromagnetic insulating state (AFI) transition. This is followed by a relatively flat region, coinciding with the stability range of the AFI phase. For $T \gtrsim 50$ K where the paramagnetic insulator (PI) regime prevails, ρ passes through a gentle maximum and then drops monotonically with rising $T > 120$ K. Note that the position of the maximum is not related to the magnetic transition. The stability ranges of the various phases are indicated at the top of the diagram. Below 30 K and above 120 K the resistivity follows the Arrhenius law: plots of $\log_{10}\rho$ vs $1/T$ are reasonably linear, with x-independent conductivity activation energies $\varepsilon_a = 300 \pm 20$ and 105 ± 10 meV below 30 K and above 120 K, respectively. The larger activation energy in the low-T regime may be due to the exchange splitting in the low-T regime. The data in the low-T regime may be fit almost equally well to a variable range hopping law for charge carriers, namely, $\log_{10}\rho \propto (T_0/T)^{1/4}$. However, unpublished magnetic susceptibility data in our laboratory are incompatible with strictly localized charge carrier models. Therefore, we ascribe the activation energy to a Mott-Hubbard gap $\varepsilon_0 \approx 2\varepsilon_a$ present in both the AFI and PI phases.

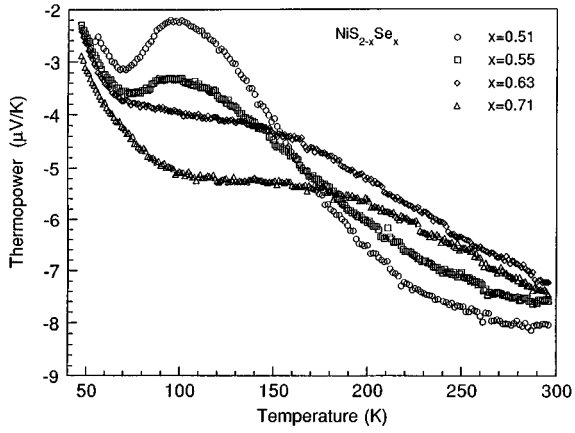

FIG. 8. Thermoelectric properties for $NiS_{2-x}Se_x$ in the composition range $0.51 \leqslant x \leqslant 0.71$.

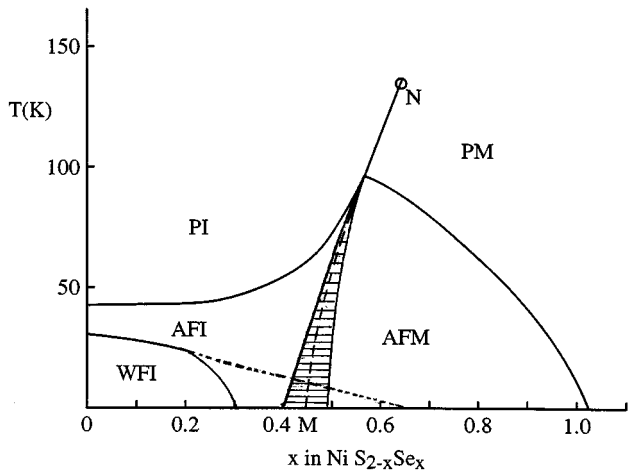

FIG. 9. Proposed composite phase diagram for the $NiS_{2-x}Se_x$ system in the range $0 \leqslant x \leqslant 1$, based on Refs. 4–7,9,13,17,20, and present results. PI=paramagnetic insulator, AFI=antiferromagnetic insulator, WFI=weakly ferromagnetic insulator (canted antiferromagnet), AFM=antiferromagnetically ordered metal, PM =paramagnetic metal. Hatched area and dotted line indicates regions where various investigators reported different findings.

In Fig. 1(b) are shown resistivity data taken by conventional four-probe techniques. The results are in essential agreement with the data of Fig. 1(a), though differences in detail remain. These do not alter the conclusions reached in Sec. IV.

(b) $0.38 \leqslant x \lesssim 0.45$: As is apparent from Figs. 2 and 3 one first encounters a range in which ρ changes little with T. According to Fig. 6(a) the resistivities of these alloys lie in the range $10^2 \lesssim \rho \lesssim 10^{-2}$ Ω cm; there is thus a trend toward metallicity with increasing x. However, for temperatures below 50 K these compounds basically still remain in the WFI/AFI regime of the phase diagram of Fig. 9. This is followed by a rapid rise of ρ with T as one approaches the AFI/PI boundary. The maximum in ρ coincides roughly with or lies slightly above the transition to the paramagnetic insulating (PI) phase. In the latter regime ρ diminishes nearly exponentially with rising T. The conductivity activation energies remain in the range of 105 ± 10 meV for all of the samples. Correlating the resistivities with the different phases is problematic: various authors differ in the precise location of the steeply rising AFI/PI phase boundary (line MN) shown in Fig. 9. Clearly, theoretical guidance is needed here to sort out the qualitative trends of the data.

Of great interest is the set of resistivities for $T < 30$ K for specimens within the range $0.38 \leqslant x \leqslant 0.45$. As is evident from Figs. 2, 3, and 6(a), ρ falls in the range of 10^{-1} to 1 Ω cm and is almost independent of T. These quasimetallic characteristics place $NiS_{2-x}Se_x$ with $0.38 \leqslant x \leqslant 0.45$ in a category between normal semiconductors and correlated metals for which $\rho \approx 10^{-3}$ Ω cm. This feature will be discussed in more detail in Sec. IV.

(c) x=0.51: These data are displayed in Fig. 4. Here $\rho \approx 10^{-3}$ Ω cm varies little with T up to 45 K. Beyond that point one again observes a very marked rise of ρ with T for the narrow temperature interval marking the corner of the AFI region in Fig. 9. The resistivity then peaks at a temperature slightly beyond the transition to the PI state and then drops rapidly with rising T. The inset shows a plot of $\log_{10}\rho$ vs $1/T$ for the data beyond 80 K. The conductivity activation energy deduced from the Arrhenius plot for this composition has now dropped to 28 meV.

(d) x=0.55, 0.58: This regime, shown in Fig. 5, top curves, still exhibits a flat maximum in the resistivity which is greatly reduced compared to those in Fig. 4. As before, at low temperatures the ρ vs T curve for this sample is characteristic of the AFM phase with a crossover to the PI (strictly speaking, semiconducting) phase. Beyond 300 K the resistivity for the sample with $x=0.58$ presumably drops with rising T, as shown in the earlier literature.[11] The vertical markers indicate the transition temperature between the low-temperature antiferromagnetic metallic (AFM) and the higher-temperature paramagnetic metallic (PM) regimes.

(e) x>0.58: Here one finally encounters the paramagnetic metallic regime; the transition from the AFM to the PM regime occurs without marked changes in $\rho(T)$, as the moment value in the AFM phase is small. The resistivity of the samples for $T<50$ K remains below 2 mΩ cm: this limit becomes progressively smaller as the composition $x=1$ is approached and ultimately falls below $\rho=10^{-3}$ Ω cm.

In conclusion, one can roughly divide the samples into three categories: (i) those for which $\rho(T)$ diminishes with T, with only a slight maximum close to the AFI-PI boundary, (ii) those with a strong maximum close to the AFM-AFI boundary, and (iii) metallic systems ($x>0.58$). We shall see next that the thermopower data fall also in those three categories; this feature of the latter data will help us in identifying the opening of a Mott-Hubbard gap, associated with carrier localization.

B. Seebeck measurements

In rationalizing the thermopower data one can, as in the previous section, distinguish several regimes: (i) for $x<0.24$ the thermopower is slightly positive and vanishes at $T=0$; (ii) for $0.24\leqslant x\leqslant 0.48$ α is negative at low and high temperature, and positive in between; and (iii) α is always negative for $x\geqslant 0.51$. The simplest interpretation of the data involving the Mott-Hubbard picture can be provided by assuming that the thermopower is metalliclike and negative when Mott-Hubbard subbands collapse at high temperatures so that a correlated metal (AF or not) is formed. By contrast, α is large and positive when the Mott-Hubbard subbands are formed in the semiconducting range, and α is also numerically small at low temperatures. The interpretation of the Seebeck coefficients α in $NiS_{2-x}Se_x$ and $Ni_{1-y}Cu_yS_2$ as provided by Adler and co-workers[11,30,31] was based on a one-band electron correlation theory described in their publications. An excellent data fit was achieved by use of this six-parameter model for temperatures in excess of the peak temperature T_m, including changes in sign at elevated temperatures. However, this approach failed to reproduce the observed drop in α with diminishing T below T_m.

IV. DISCUSSION

As anticipated, with increasing x, $NiS_{2-x}Se_x$ moves towards metallicity but exhibits clear correlated metallic characteristics at all temperatures only for $x\geqslant 0.58$. A similar trend is observed in the $(V_{1-x}Ti_x)_2O_3$ system[32,33] with increasing Ti content, although in the latter case the resistivity changes at the metal-insulator transition are discontinuous. For $NiS_{2-x}Se_x$ the most spectacular changes in resistivity (although continuous) are displayed in Figs. 3 and 4; these take place when with rising temperature the system transforms to the AFI phase. The sharp, though continuous, rise in $\rho(T)$ is attributed to the opening of a Mott-Hubbard gap at the boundary. This interpretation is supported by two facts. First, the gap opens up as the temperature rises; this change cannot be ascribed to the opening of a Slater gap associated with the AFM to AFI transition, since the crystal symmetry remains the same across the transition. Second, the continuous increase of $\rho(T)$ across the phase boundary means that electron correlations, not a discontinuous change of the magnetic-moment magnitude, provide the main contribution to the gap. However, a decisive test of our interpretation would be provided by Hall-coefficient measurements in that regime, since in the case of the Mott localization the carrier mass should increase remarkably near the transition,[34–38] while leaving the carrier-concentration constant.

The sharp rise in resistivity in the temperature interval 50–100 K cannot be interpreted as due to the spin-disorder scattering. This is because the transition for appropriately synthesized samples[20] is of first order, indicating that magnetic fluctuations near the transition are negligible. The resistivity peak is simply far too wide to be associated with any scattering in a critical magnetic regime.

We emphasize again that the $NiS_{2-x}Se_x$ system is unusual in that, even when the metallic configuration is stable at low temperature, the system is driven toward a more insulating state with rising temperature in the range 50–100 K. This counterintuitive behavior must reflect the opening up of a gap which is the result of a change in the nature of the electronic states, since the magnetic ordering is of the same character on both sides of the transition. A trace of this type of behavior is fund even for relatively low x, where the insulating state is stable at all temperatures. The fundamental reason for this changeover is provided by the near compensation of negative band energy (relative to particle localization) of itinerant $3d$ electrons, and the positive repulsive interaction between them, as described in detail elsewhere.[35–38] The entropy of itinerant electrons in the Fermi-liquid (metallic) state is small (at low T) compared to the entropy change of the same electrons in the localized-moment (insulating) configuration. Thus, with rising T, the entropy gain achieved by localization drives the metal-insulator transition.[35–38] The usual AFI→PI transition takes place at higher temperatures. The second important factor of the Mott localization is the reentrant metallic behavior reached in the high-temperature regime in a continuous manner. Such behavior must always be observed, since ultimately the entropy of the Fermi-liquid state is higher than that of localized spins as the high-temperature limit is approached ($k_B\ln 4$ and $k_B\ln 2$, respectively, per electron, where k_B is the Boltzmann constant).

One additional basic feature of the data displayed collec-

tively in Fig. 6(a) should be analyzed. Namely, in the concentration range x between 0.38 and 0.44 a quasimetallic state is observed at low temperatures, with resistivities in the range 0.1–1 Ω cm, i.e., well above the Mott limit for the normal metallic state. These resistivities are nearly constant down to the lowest temperature of the measurements. Furthermore, the quasimetallic state is well defined, since it is also reached in the high-temperature regime, after peaking around 70 K. We regard this quasimetallic behavior as a manifestation of the *semimetallic antiferromagnetic state*. This state will be discussed in detail separately.[40] We only mention that the Slater splitting in the AFM phase cannot be complete since the cationic sublattice has the fcc structure. Therefore, there must be at least some points on the Fermi surface, where the Slater gap vanishes. In such a situation the antiferromagnetic semimetallic (AFSM) state transforms into the AFI phase at the transition. The Mott-Hubbard gap thus created is isotropic, being generated by the intra-atomic interaction. The usual magnetic (AFI→PI) transition takes place at still higher temperature.

With regard to the Seebeck coefficient one should note the crossover or near crossover in the sign of α at low temperatures and again at high temperatures. Though the data for $x=0$ and 0.24 were not taken to sufficiently high temperatures to show the second sign change, the trends in Fig. 7 correspond well with those displayed in Ref. 11, where a crossover was reported in the 400–500 K range. We observe that in the intermediate temperature range of the PI phase the Seebeck coefficient is positive and large, as is consistent with a band structure which has split into Mott-Hubbard subbands. At very high temperatures, where k_BT becomes comparable to the band gap, the Seebeck coefficient is expected to decline to values consistent with those encountered experimentally at $T>150$ K in Fig. 7 and to those reported in Ref. 11 for larger x at $T>300$ K.

By contrast, in the low-T range where the WFI and AFI phases are stable, α is small under conditions where this quantity should normally be large. This strongly suggests that in this range a two-band model is appropriate for the interpretation of the data. It may be shown through standard thermodynamic arguments[39] that the Seebeck coefficient of a material in which electron and hole conduction occurs concurrently is given by

$$\alpha=(-\sigma_n\alpha_n+\sigma_p\alpha_p)/\sigma, \quad \sigma\equiv\sigma_n+\sigma_p\equiv 1/\rho,$$

where α_n and α_p are the partial conductivities due to electron and holes, respectively, and $\alpha_n,\alpha_p>0$ are the corresponding partial Seebeck coefficients. In the AFM state the two-band picture is realized by the partly split Slater subbands.

One check on the efficacy of this model is to utilize the experimental α and ρ values and to plot $\alpha/\rho=-\alpha_n\sigma_n+\alpha_p\sigma_p$ vs T; the calculations for $0\leqslant x\leqslant 0.44$ and $0.51\leqslant x\leqslant 0.71$ are displayed in Figs. 10(a) and 10(b). These results provide evidence in favor of the hypothesis: at low $T\leqslant 150$ K, α/ρ is close to zero in all cases, showing that the contributions $-\alpha_n\alpha_n$ and $\alpha_p\alpha_p$ are nearly in balance; i.e., the samples are intrinsic. For samples with $x=0$, 0.1, and 0.2 the data of Ref. 11 show a similar trend. At more elevated

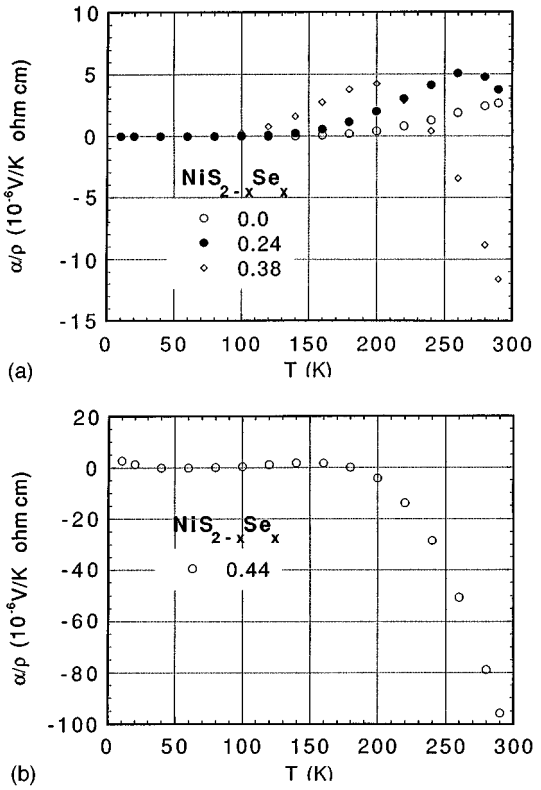

FIG. 10. Plots of α/ρ vs T as a test for the two-band conduction model. See text. (a) $x=0$, 0.24, 0.38; (b) $x=0.44$.

T there is an increasing imbalance in $\alpha_p\sigma_p$ vs $\alpha_n\sigma_n$, and in the PI regime the hole contribution dominates the electron contribution.

The maximum thermopower for $x\leqslant 0.44$ corresponds roughly to the maximum in resistivity, the presence of which we have attributed to the opening of the Mott-Hubbard gap in the spectrum. The hole contribution from the lower Hubbard subband must exceed that of electrons excited to the upper subband, whereas for $x\geqslant 0.61$ the split-band picture ceases to hold and the contribution is mainly n type. It is clear that in the whole range of concentration, where the MIT appears, the electron and hole contributions to the thermopower almost compensate each other. However, this two-carrier interpretation of transport requires further careful analysis to incorporate the antiferromagnetic semimetallic state mentioned earlier.

Last, in the regime where the system tends towards metallicity, one anticipates[35] that $|\alpha|$ should be numerically small and should increase linearly with rising temperature. This is indeed the situation for the data displayed in Fig. 8 at $T\geqslant 150$ K.

It should be noted that the pyrite structure remains basically unaffected by the various phase transitions indicated in Fig. 9: there is no indication of either a broadening or a splitting of the x-ray-diffraction peaks in the range from 4.2 to 300 K.[22] The present results therefore can be understood in terms of electron correlation phenomena in the absence of conspicuous lattice distortions. As already mentioned, these alterations are achieved solely by substitution of Se for S, while the Ni cation lattice is left intact. Nonetheless, further studies are required to locate more precisely the transition temperatures between various phases marked in Fig. 9.

ACKNOWLEDGMENTS

The authors wish to thank P. A. Metcalf for advice concerning the preparation of the single crystals. This research was supported by NSF Grant No. DMR 92-22986 at Purdue University, West Lafayette, IN; at Northwestern University, Evanston, IL, T.H. was supported on NSF Grant No. DMR 92-22245; in this work use was made of the MRL Central Facilities supported by NSF Grant No. DMR 91-20521. J.S. was supported in part by NSF Grant No. INT 93-08323 in the USA, and by KBN grants in Poland.

*Present address: Beckman Institute, University of Illinois, 405 N. Matthews Ave., Urbana, IL 61801.

† Permanent address.

[1] J. A. Wilson and G. D. Pitt, Philos. Mag. **23**, 1297 (1971).

[2] D. D. Klemm, N. Jahr. Miner. Monat. **1962**, 32.

[3] R. J. Bouchard, J. L. Gillson, and H. S. Jarrett, Mater. Res. Bull. **8**, 489 (1973).

[4] H. S. Jarrett, R. J. Bouchard, J. L. Gillson, G. A. Jones, S. M. Marcus, and J. F. Weiher, Mater. Res. Bull. **8**, 877 (1973).

[5] F. Gautier, G. Krill, M. F. Lapierre, and C. Robert, Solid State Commun. **11**, 1201 (1972); J. Phys. C **6**, L320 (1973).

[6] G. Krill, M. F. Lapierre, F. Gautier, C. Robert, G. Czjzek, J. Fink, and H. Schmidt, J. Phys. C **9**, 761 (1976).

[7] F. Gautier, G. Krill, M. F. Lapierre, P. Panissod, C. Robert, G. Czjzek, J. Fink, and H. Schmidt, Phys. Lett. **53A**, 31 (1975).

[8] P. Plumier and G. Krill, J. Phys. Lett. **36**, L249 (1975).

[9] G. Czjzek, J. Fink, H. Schmidt, G. Krill, M. F. Lapierre, P. Pannisod, F. Gautier, and C. Robert, J. Magn. Magn. Mater. **3**, 58 (1976).

[10] S. Ogawa, J. Appl. Phys. **50**, 2308 (1970).

[11] P. Kwizera, M. S. Dresselhaus, and D. Adler, Phys. Rev. B **21**, 2328 (1980).

[12] G. Krill and A. Amamou, J. Phys. Chem. Solids **41**, 531 (1980).

[13] H. Takano and A. Okiji, J. Phys. Soc. Jpn. **50**, 3835 (1981).

[14] T. Miyadai, S. Sudo, Y. Tazuke, N. Mōri, and Y. Miyako, J. Magn. Magn. Mater. **31-34**, 337 (1983).

[15] N. Mōri, M. Kamada, H. Takahashi, G. Comi, and S. Susaki, *Solid State Physics Under Pressure: Recent Advance with Anvil Devices, Izu-Nagaoka, Japan, 1984* (Reidel, Dordrecht, 1985), p. 247.

[16] S. Sudo and T. Miyadai, J. Phys. Soc. Jpn. **54**, 3934 (1985).

[17] S. Sudo, T. Nishioka, Y. Miyako, and T. Miyadai, J. Phys. Soc. Jpn. **55**, 1806 (1986).

[18] T. Miyadai, Y. Tazuke, S. Kinouchi, T. Nishioka, S. Sudo, Y. Miyako, K. Watanabe, and K. Inoue, J. Phys. (Paris) Colloq. **C8-49**, 187 (1988).

[19] T. Miyadai, M. Saitoh, and Y. Tazuke, J. Magn. Magn. Mater. **104-107**, 1953 (1992).

[20] S. Sudo, J. Magn. Magn. Mater. **114**, 57 (1992).

[21] X. Yao and J. M. Honig, Mater. Res. Bull. **29**, 709 (1994).

[22] X. Yao, S. N. Ehrlich, G. Liedl, and J. M. Honig, *The Metal-Nonmetal Transition Revisited*, edited by P. P. Edwards and C. N. R. Rao (Taylor & Francis, London, 1995), p. 127 ff.

[23] D. S. Jin, A. Husmann, Y. Zastavker, T. F. Rosenbaum, X. Yao, and J. M. Honig (unpublished).

[24] K. Kourtakis, J. DiCarlo, R. Kershaw, K. Dwight, and A. Wold, J. Solid State Chem. **76**, 186 (1986).

[25] S. Fiechter and H.-M. Kuhn, J. Cryst. Growth **83**, 517 (1987).

[26] J. G. Fleming, J. Cryst. Growth **92**, 287 (1988).

[27] L. J. van der Pauw, Philips Res. Rep. **13**, 1 (1958).

[28] H. O. Marcy, T. J. Marks, and C. R. Kannewurf, IEEE Trans. Instrum. Meas. **32**, 756 (1990); this program also made use of the SB100 thermopower control system provided through the courtesy of MMR Technologies Inc., Mountain View, CA.

[29] P. M. Chaikin and J. F. Kwak, Rev. Sci. Instrum. **46**, 28 (1975).

[30] E. J. Yoffa and D. Adler, Phys. Rev. B **12**, 2260 (1975).

[31] A. K. Mabatah, E. J. Yoffa, P. C. Eklund, M. S. Dresselhaus, and D. Adler, Phys. Rev. Lett. **39**, 494 (1977); Phys. Rev. B **21**, 1676 (1980).

[32] S. A. Shivashankar and J. M. Honig, Phys. Rev. B **28**, 5695 (1983).

[33] S. A. Carter, J. Yang, T. F. Rosenbaum, J. Spałek, and J. M. Honig, Phys. Rev. B **43**, 607 (1991).

[34] S. A. Carter, T. F. Rosenbaum, P. Metcalf, J. M. Honig, and J. Spałek, Phys. Rev. B **48**, 16 841 (1983).

[35] J. Spałek, J. M. Honig, M. Acquarone, and A. Datta, Magn. Magn. Mater. **54-57**, 1047 (1986).

[36] J. Spałek, A. Datta, and J. M. Honig, Phys. Rev. Lett. **59**, 778 (1987).

[37] A. Datta, J. M. Honig, and J. Spałek, Phys. Rev. B **44**, 8459 (1991).

[38] For review see J. Spałek, J. Solid State Chem. **38**, 70 (1990); J. Spałek and W. Wojcik, in *Spectroscopy of Mott Insulators and Correlated Metals*, edited by A. Fujimori and Y. Tokura, Springer Series in Solid State Sciences Vol. 119 (Springer-Verlag, Berlin, 1995).

[39] T. C. Harman and J. M. Honig, *Thermoelectric and Thermomagnetic Effects and Applications* (McGraw-Hill, New York, 1967), Chap. 3.

[40] J. Spałek, J. M. Honig, and T. F. Rosenbaum (unpublished).